THE JOURNAL OF PHYSICAL CHEMISTRY LETTERS
A JOURNAL OF THE AMERICAN CHEMICAL SOCIETY

pubs.acs.org/JPCL Letter

Efficient 2D to 0D Energy Transfer in HgTe Nanoplatelet-Quantum Dot Heterostructures through High-Speed Exciton Diffusion

Stephanie M. Tenney,[§] Lauren A. Tan,[§] Xuanheng Tan, Mikayla L. Sonnleitner, Belle Coffey, Jillian A. Williams, Ricky Ronquillo, Timothy L. Atallah, Tasnim Ahmed, and Justin R. Caram*

Cite This: *J. Phys. Chem. Lett.* 2023, 14, 9456−9463 Read Online

ACCESS | Metrics & More | Article Recommendations | Supporting Information

ABSTRACT: Large area absorbers with localized defect emission are of interest for energy concentration via the antenna effect. Transfer between 2D and 0D quantum-confined structures is advantageous as it affords maximal lateral area antennas with continuously tunable emission. We report the quantum efficiency of energy transfer in in situ grown HgTe nanoplatelet (NPL)/quantum dot (QD) heterostructures to be near unity (>85%), while energy transfer in separately synthesized and well separated solutions of HgTe NPLs to QDs only reaches 47 ± 11% at considerably higher QD concentrations. Using Kinetic Monte Carlo simulations, we estimate an exciton diffusion constant of 1−10 cm^2/s in HgTe NPLs, the same magnitude as that of 2D semiconductors. We also simulate in-solution energy transfer between NPLs and QDs, recovering an R^{-4} dependence consistent with 2D-0D near-field energy transfer even in randomly distributed NPL/QD mixtures. This highlights the advantage of NPLs 2D morphology and the efficiency of NPL/QD heterostructures and mixtures for energy harvesting.

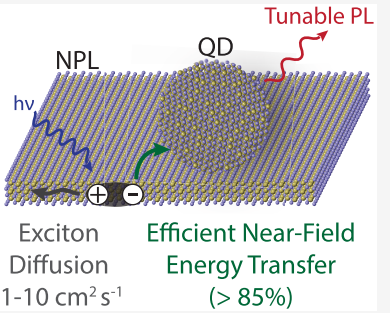

Antennas collect diffuse excitation and concentrate it at a localized receiver, allowing for a separation between energy collection and localized transformation. Converting diffuse and low intensity light into localized emitters limits parasitic reabsorption and is crucial to waveguiding and solar concentration applications. Such behavior has been leveraged across material systems, including natural and artificial photosynthetic systems, organic photovoltaics, self-assembled light-harvesting nanotubes, and quantum dot heterostructures typically involving the funneling of excitons from a large collection area to a bright emitter or reaction center.[1−6]

One such class of materials that may be leveraged as an optical antenna are semiconductor nanoplatelets (NPLs); these are colloidal nanocrystals that have been primarily studied for their optoelectronic properties afforded by their unique two-dimensional morphology including large absorption cross sections, high quantum yields, directed emission, and large exciton binding energies.[7−10] NPLs are often classified by number of monolayers (ML) where one ML is one layer of MX where M = Cd, Hg and one of X = S, Se, and Te and commonly range from 2 to 5 ML thick. Although their thickness is only a few nanometers, their lateral extent can range tens to hundreds of nm and have recently been demonstrated to micron scale.[11] For this reason, NPLs are promising antennas due to their large lateral faces and high absorption cross sections for exciton collection. In addition, they offer the advantage of bandgap tuneability and broad absorption across visible and near-infrared spectral regions.[7,12,13] However, they require the appropriate acceptor in order to concentrate energy to a single point.

We focus our attention to our previously reported HgTe NPL/quantum dot (QD) heterostructures where we observed efficient energy transfer from NPL to QD derived *from the same material*.[14] Other reports in the literature have shown energy transfer to QDs in dot-on-nanoplatelet heterostructures such as CdSe/ZnS, PbSe/CdSe, CdSe/PbSe, and CdSe/Au clusters.[15−18] We believe that the high efficiency of our HgTe/QD systems arises from the fact that the NPL antenna and QD acceptor have identical compositions but differing confinement. This arrangement works only because the HgTe NPL is in a highly confined regime of only a few monolayers, while the QD confinement is continuously tunable.

In our prior work, we hypothesized that our emissive heterostructures relied on long-range exciton transport in the NPL followed by near unity energy transfer to the QD. We based this supposition by considering the average lateral lengths of the NPLs (~500 nm), the apparent high quantum yield of the emissive heterostructures (>30% at the QD bandgap accompanied by complete quenching of the NPL emission), and the extremely low number density of QDs contributing to the absorption cross-section. These results qualitatively implied that excitons must be sampling a large

Received: August 3, 2023
Accepted: October 9, 2023
Published: October 13, 2023

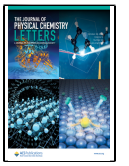

https://doi.org/10.1021/acs.jpclett.3c02168
J. Phys. Chem. Lett. 2023, 14, 9456−9463

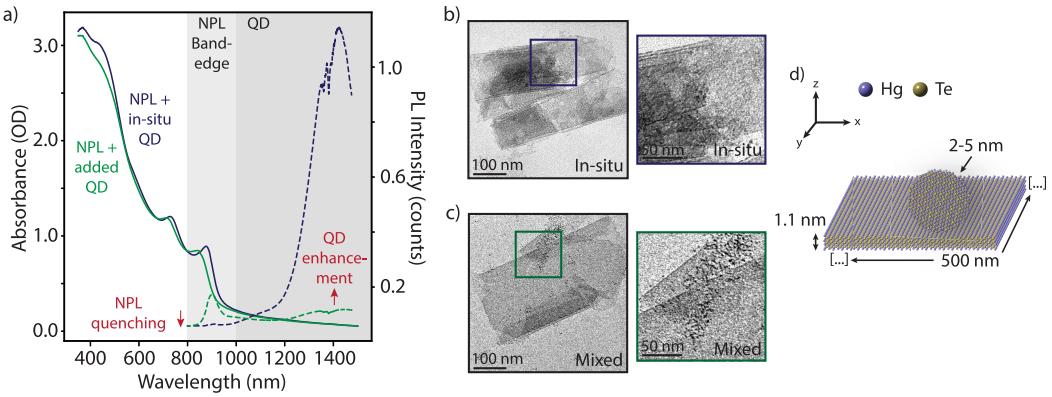

Figure 1. (a) Representative spectra demonstrating the enhancement in photoluminescence when HgTe QDs are grown via an in situ QD/NPL heterostructure compared to those simply mixed with NPLs. The in situ heterostructure experiences complete band-edge quenching, suggesting energy transfer. (b-c) TEM showing in situ and mixed systems of HgTe NPLs and QDs. (d) A schematic of QD on NPL where the QD is in close contact with the NPL. Note that the ligands are not shown for clarity.

area of the NPL before being quenched by transfer into "rare" QD on the surface.

In this work, we conduct a more systematic set of experiments and controls to understand 2D-0D energy transfer. Briefly we:

1) Reproduce the highly efficient energy transfer for in situ grown QDs, and quantify exciton quantum efficiencies,
2) Generate bounds for the number density of in situ grown and separately synthesized/mixed QDs and NPLs, and use this to inform a model of exciton diffusion and transport,
3) Compare the energy transfer to an analogously synthesized NPL QD mixture as a control experiment,
4) Determine/derive both exciton diffusion constant within an NPL, and the efficiency of energy transfer between large finite NPLs and QDs in solution,
5) Contextualize exciton diffusion and 2D-0D energy transfer across many material systems.

Taken together, these results demonstrate the role that near-field energy transfer can play in allowing for extremely efficient excitation energy transfer in NPL systems, and extended NPLs may act as excellent antennas.

In Situ Grown HgTe NPL/QD Heterostructure. We previously found that HgTe QDs will grow on the surface of HgTe NPLs following a cation and ligand exchange from oleic acid passivated CdTe NPLs to oleylamine passivated HgTe.[14] The growth can be controlled by precursor concentrations and is temperature activated—holding the cation-exchanged NPLs at elevated temperatures will speed up growth and storing in a freezer will inhibit growth. This growth is specific to HgTe because QDs will form at ambient temperatures with the same precursors required for cation exchange.[19] These in situ grown HgTe QDs appear to be attached to the surfaces of the NPLs, possibly growing epitaxially from reactive sites introduced by the labile surface Hg, and result in near complete NPL band-edge quenching along with high photoluminescence quantum yield (PLQY) from the resultant HgTe quantum dots (Figure 1a-b, blue trace). Our prior work showed that HgTe energy transfer is occurring from NPL to QD and allows for a continuously tunable Stokes shift depending on the bandgap of the QD. We previously showed that the PLQY of the QD grown through this method is very high, with values from ~30−50%.[14] These results are comparable to some of the highest PLQY reported for HgTe QDs and suggests that the transfer must be near unity.[19]

Estimate of In Situ Donor−Acceptor Number Density. To give an estimate for the ratio of donor to acceptor, we calculate the concentration of both the NPLs and QDs in the in situ heterostructure in the Supporting Information (Section S2). Briefly, an upper bound on the NPL concentration can be estimated from their average size and amount of precursor used in synthesis, assuming a 100% reaction yield for all steps, including cation exchange. We observe very little change in the absorption spectra of the NPLs after the HgTe QDs have grown and show photoluminescence (PL), indicating that the QD growth occurs at low concentrations relative to that of the NPLs. To estimate the QD concentration, we found the difference in absorption at the QD band edge between a fresh NPL sample (no QD growth) and an aged NPL sample with QD growth (Figure S2). We then used the absorption cross section to give an estimate of the QD concentration and found <5 QDs per NPL for all of the in situ samples we collected (Table S1).

Ex Situ Mixed HgTe NPLs and QDs. For comparison to in situ NPL/QD heterostructures, we perform a control experiment by first separately synthesizing oleylamine passivated HgTe QDs with sizes that match the in situ grown QDs (Figure S1) and then mix a comparable concentration with 3 ML HgTe NPLs isolated immediately after cation exchange (further details in S3). Hereafter we will refer to this sample as mixed NPLs and QDs. While we are able to reproduce energy transfer by mixing QDs and NPLs, there is less quenching of the band edge emission (Figure 1a, green trace), suggesting lower efficiencies of transfer. From TEM, we observe in situ grown QDs in contact with the surface of the NPLs that are not washed away during centrifugation, while the mixed QDs are easily removed using gentle centrifugation, which recovers NPL band edge PL (Figure 1c and Figure S5). We predict that the in situ grown quantum dots are epitaxially attached or in very close proximity to the NPLs in the heterostructure (Figure 1d), which affords it such high energy transfer efficiencies compared to separately synthesized QDs and NPLs which are likely not adsorbing to the NPL surfaces and thus constitute an "ideal" solution. The in situ NPL/QD heterostructure not only allows for slow controlled growth of a low concentration of high PLQY QDs, but also overcomes distance limitations of energy transfer

https://doi.org/10.1021/acs.jpclett.3c02168
J. Phys. Chem. Lett. 2023, 14, 9456−9463

systems when the donor and acceptor are synthesized separately.

The Quantum Efficiency of Energy Transfer. To determine the experimental quantum efficiency (QE) of transfer, we collected absorbance and PL measurements while exciting the system at different wavelengths. We excite both mixed and in situ 3 ML NPL and QD at 750 nm to observe energy transfer (donor plus acceptor) and isolate the QD (acceptor only) by exciting at 950 nm, below the band-edge of the NPL near 880 nm (Figure 2a). After normalizing

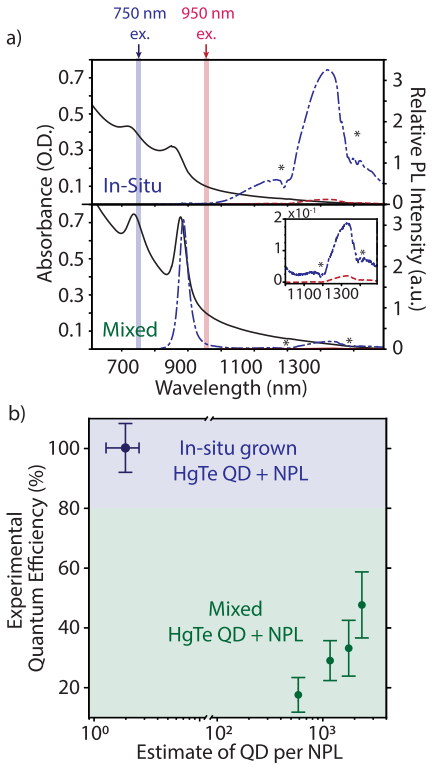

Figure 2. (a) The absorption (solid line) and emission (dashed line) spectra of in situ grown HgTe QDs + NPLs and mixed QDs + NPLs. Both samples are excited above and below the NPL bandgap (750 and 950 nm, respectively) to excite the donor + acceptor and acceptor only. The inset highlights the difference in PL intensity between the in situ and mixed heterostructures. The (*) indicates regions of C−H stretch reabsorption from the hexanes solvent. All subsequent quantum efficiency values reported are collected in hexanes, but a comparison to TCE is given in the Supporting Information. (b) The quantum efficiency (QE) of energy transfer is calculated for both systems. The mixed system is evaluated at increasing concentrations, while the in situ QE is calculated and the number of QD per NPL is estimated from the spectra. All data points are a result of the mean of multiple trials, and the error is calculated through the standard error of the mean.

PL by excitation power, this allows us to observe an enhancement in QD PL when exciting into the NPL bandgap. The absorbances of NPL and QD must be noted at both excitation wavelengths, so we use a sample of NPLs only (no QDs present) and QDs only (no NPLs present). The emission at 750 nm (Em_{750}) when exciting both NPL and QD can be expressed as

$$Em_{750} = Abs_{QD,750} * QY_{QD,750} + Abs_{NPL,750} * QE_{ET} * QY_{QD,750} \quad (1)$$

where Abs_{QD} is the absorbance of the QD, QY_{QD} is the PLQY of the QD, Abs_{NPL} is the absorbance of the NPL, and QE_{ET} is the quantum efficiency of energy transfer. Similarly, when exciting only the Q:

$$Em_{950} = Abs_{QD,950} * QY_{QD,950} + Abs_{NPL,950} * QE_{ET} * QY_{QD,950} \quad (2)$$

We will assume a negligible contribution from the sub-band states in the donor (NPL) despite the presence of an Urbach tail in HgTe NPLs. We rule out a significant contribution to the overall PL from exciting into these states in Figure S6. The emission of acceptor only then becomes

$$Em_{950} = Abs_{QD,950} * QY_{QD,950} \quad (3)$$

Note that we are assuming that the quantum yield of the acceptor does not change by the presence of the donor and is also independent of excitation wavelength. We can then use the total integrated emission along with the absorption spectra to calculate the quantum efficiency of energy transfer (QE_{ET}) by

$$QE_{ET} = \frac{\frac{Em_{750}}{Em_{950}} * Abs_{QD,950} - Abs_{QD,750}}{Abs_{NPL,750}} \quad (4)$$

We repeated the experiment on many different samples and found that overall, the QE of transfer for the in situ case is always higher than the control case, from >85% compared to the mixed case of 35−63%. The average experimental QEs of multiple trials are reported in Figure 2b (black data points), along with their standard errors of the mean. For the mixed system, we started at low concentrations of added QDs and found that we were not able to observe energy transfer until we reached the concentrations shown above. Even with this much higher ratio of QD per NPL, we were not able to cross the QE threshold that we observed in the in situ case. We observed that the QE scales with concentration likely because these QDs experience energy transfer through FRET rather than near-field as in the in situ case (Figure 2b). Therefore, the energy transfer is proportional to the average distance between particles, which scales with concentration.

Modeling of FRET Efficiency. To explain the energy transfer, we employed a Förster resonance energy transfer (FRET) model. This yielded an estimated efficiency of energy transfer (>20%) that is significantly higher than the quantum yield of the donor alone (5−10%). The result is unusual as simplistically FRET is assumed to be bounded by QY of the donor (at low quantum yields); however, this has proved to be an oversimplification both theoretically and experimentally.[20] In our case, this apparent mismatch prompted a more detailed study of the FRET mechanism for our specific NPL-QD system.

Following the work by Chuang et al., we first developed a more specific model for our 2D (NPLs) to 0D (QDs) energy transfer system, which takes the scale of donor−acceptor distances and the actual geometry of the dipole distribution into consideration.[21] Briefly, the relatively small HgTe QD is modeled as one single dipole, while the larger HgTe NPL

https://doi.org/10.1021/acs.jpclett.3c02168
J. Phys. Chem. Lett. 2023, 14, 9456−9463

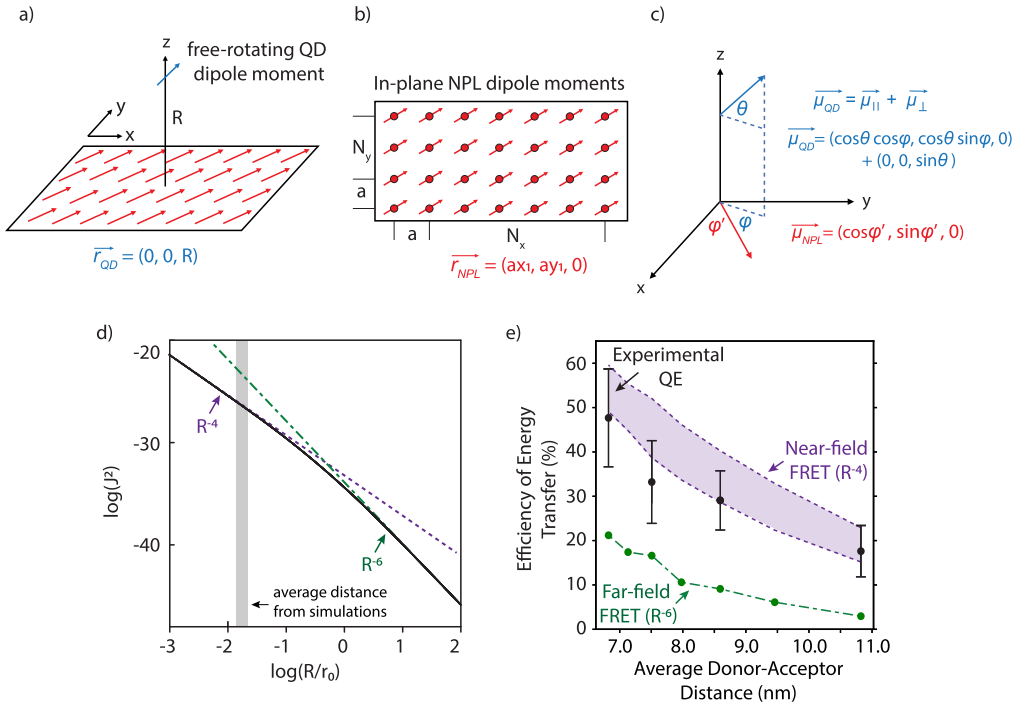

Figure 3. Model for studying the distance dependence of the NPL-QD FRET system. (a) QD with a free-rotating dipole moment (blue vector) and NPL consisting of individual in-plane dipole moments (red vectors). The position vector of QD dipole is given in terms of Cartesian coordinates. (b) Top-down view of the in-plane dipole moments of the NPL. The position vector of NPL dipoles is given in Cartesian coordinates. (c)Diagram of altitude angle and azimuth angles for dipole moments. The "dipole vectors" are given in spherical coordinates. (d) The distance dependence of the FRET rate, plotted on a log−log scale to extract the index of R. The average donor−acceptor distances found in our simulations are indicated by the gray box. (e) The comparison of our experimental energy transfer efficiencies (black) to simulated results for both the near-field (purple) and far-field limit of FRET (green). The near-field results are represented as a range due to error (discussed in Supporting Information), whereas the error on the far-field results is too low to be shown in the plot.

consists of multiple dipoles (Figure 3a−c). The FRET rate equation is determined by calculating the summation of dipole−dipole coupling of donor−acceptor pairs over all possible dipole orientations (see Supporting Information for details). The summation can be calculated as a continuous integration to extract the distance dependence:

$$k_{\mathrm{FRET}} \propto \begin{cases} \dfrac{3\pi^3}{8r_0^2}\left(1+\dfrac{1}{\pi}\right)\dfrac{1}{R^4} & R \ll r_0 \\ \dfrac{\pi^3}{4}\left(5-\dfrac{3}{\pi}\right)\dfrac{1}{R^6} & R \gg r_0 \end{cases} \tag{5}$$

where R is the distance between QD and NPL and r_0 is the size of the NPL. The traditional R^{-6} distance dependence is recovered at the far-field limit, but in the case of near-field FRET, the rate equation has a different distance dependence and prefactor. This behavior is also shown through numerical calculation, where a transition of R^{-4} to R^{-6} dependence can be clearly seen with increasing donor−acceptor distances (Figure 3d). Considering the high QD-to-NPL ratio and the relatively large size of the NPL, it is likely that the traditional (R^{-6}) FRET rate equation fails to accurately describe the situation, and it is necessary to use the near-field FRET rate equation. We then used the obtained near-field FRET rate equation in kinetic Monte Carlo simulations to calculate the FRET efficiencies for different QD concentrations (see Supporting Information Section S7 for details). Based on the simulations, we can confirm that the donor−acceptor distances are indeed in the near-field range where the R^{-4} dependence should be used. The average distance depends on the QD-NPL ratio, but we found these R/r_0 distances to be between 0.0136−0.0216 (shown on a log scale in Figure 3d). By comparing the simulations with the experimental results (Figure 3e), we can conclude that the near-field FRET is indeed the energy transfer mechanism in the mixed case. Additional passivation through added ligand (1% w/v% oleylamine in hexanes solvent) before mixing improved the QE by ensuring that all nanocrystals remained suspended in solution during the measurements and passivated surface defects, which might affect either nanocrystal (a comparison to no added ligand is given in Figure S10). We also attempted to conduct the measurements in tetrachloroethylene (TCE) to avoid significant solvent reabsorption but found that this solvent reduced the QE (1−15% for mixed case and 36% for in situ case, full results in Figure S10) and dissolved the nanocrystals after a few hours, likely by the difference in solvent polarity compared to hexanes. Therefore, the values that we report in Figure 2b are all collected in hexanes. Overall, these results highlight the advantage of in situ grown QDs as having near complete transfer from the large area NPLs, establishing an efficient energy harvesting system.

The high efficiency of energy transfer is consistent with our previous expectation that the in situ grown QDs are adsorbed or in contact with the surface. It is therefore not surprising that the in situ case has a much higher QE than the mixed case given the distance between donor and acceptor. What is surprising, however, is that the number density of QDs is very low while still reaching near unity transfer. This suggests that there must be long-range exciton transport for nearly every

https://doi.org/10.1021/acs.jpclett.3c02168
J. Phys. Chem. Lett. 2023, 14, 9456−9463

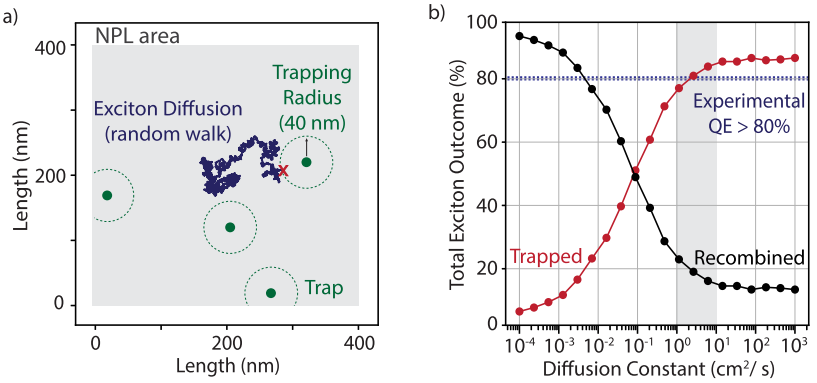

Figure 4. a) 2D random walk model of exciton diffusion over a square sheet representing a NPL. The traps shown in green represent QDs on the surface and will quench the exciton when it falls within the trapping radius. b) The results of the Monte Carlo simulation showing the percentage of excitons that trapped (red) and the percentage of excitons that recombined (black). The dashed line is the QE threshold for experimental percentage of trapped excitons.

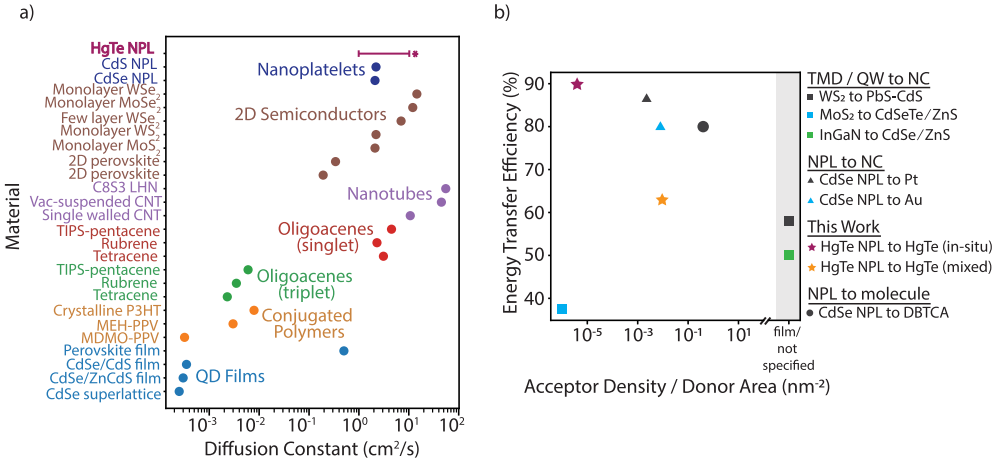

Figure 5. a) Literature diffusion constants reported for QD films,[23−26] conjugated polymers,[27,28] oligoacene triplets and singlets,[29] nanotubes,[30−32] 2D semiconductors,[33−40] and nanoplatelets[41,42] at room temperature. b) Energy transfer efficiency rates for 2D to 0D systems including TMDs and quantum well (QW) to NCs,[3,43,44] NPLs to NCs,[18,45] our results, and NPLs to conjugated fluorophores.[46]

exciton to reach a QD. Even the small-to-averaged sized NPLs represent a ∼1000−2500 nm^2 area that the exciton must sample before reaching a QD, and this must outpace the recombination rate. We therefore became interested in exploring exciton diffusion through modeling to better understand transport within these NPLs.

Modeling of Exciton Diffusion. Experimentally we observe that the energy transfer from NPL to QD results in >85% quenching. Using a Monte Carlo simulation, we determine a theoretical diffusion constant by modeling an exciton on an NPL with a two-dimensional (2D) random walk (Figure 4a). This model asserts that the movement of the excitons is diffusive rather than ballistic at room temperature, as is consistent with prior work on exciton transport in 2D materials.[22] In our model, the exciton is allowed one of two outcomes: it will either recombine according to the time scale of the experimental total photoluminescence lifetime (Figure S12), or it will undergo energy transfer by reaching a position within a radius of a trap (set to be the exciton Bohr radius in bulk HgTe, 40 nm although this is discussed further in Section S12). In all simulations, the exciton is confined to a square 2D area which can vary but follows a normal distribution centered at 500 nm—the average size of a 3 ML HgTe NPL (Figure S12). We estimate the trap density to be about 2 traps/NPL (see prior discussion and Supporting Information S2), and each NPL is given a Poissonian number of traps distributed randomly across the 2D sheet (Figure S12). Additional examples of random walks at different diffusion constants are shown in Figure S14.

We observe that in order to reach greater than 80% trapping (or the minimum experimental QE from NPL to QD), the diffusion constant of the exciton can be conservatively estimated to be between 1 and 10 cm^2/s (Figure 4b). The trapped exciton population percentage has a nonzero minimum that depends on the average number of traps per NPL—because they are placed randomly, this represents the excitons that are immediately quenched by being placed within the radius of the trap during initialization of the walk. We also observe a maximum trapping at 86% and saturation at 10 cm^2/s, which reflects the population of NPLs which have no traps (i.e., the excitons on these NPLs will always recombine). The saturation would reach 100% quenching only if every NPL has at least one trap. Although we show the results of a Poissonian distribution of traps, we also calculate the diffusion constant from a uniform number of traps/NPL in Figure S13b.

Comparison to Other Diffusion Constants and Other 2D-0D Heterostructures. Finally, in Figure 5 we compare the theoretical diffusion constant (indicated by an asterisk) to

https://doi.org/10.1021/acs.jpclett.3c02168
J. Phys. Chem. Lett. 2023, 14, 9456−9463

other excitonic materials of interest for optoelectronic applications. Diffusion constants have been studied in organic and inorganic semiconductors such as conjugated polymers, oligoacenes, and 2D TMDs, but literature results in NPLs are limited to small CdSe and CdS. Although we report an estimate, we can compare the order of magnitude from our result for HgTe to different materials and find that NPLs, despite being colloidal nanocrystals, are most comparable to the 2D TMDs, highlighting their similarity to extended 2D semiconductors. NPLs' large areas and exciton diffusion constants are essential for their antenna functionality, and although they draw the strongest comparison to 2D materials, they have the advantage of being extremely good emitters. 2D TMDs commonly have low PLQY after exfoliation (<1 to 6%) due to surface defects and require significant efforts to boost the PLQY, such as with superacid treatment.[47,48] NPLs on the other hand offer high PLQY after synthesis (~10% here for HgTe NPLs) and have access to milder solution-based treatments like passivation or shelling to minimize defects and reach near unity PLQY. They present a promising path forward toward large area semiconductors for energy collection antennas.

Many other antenna systems have demonstrated extremely high energy transfer efficiencies such as photosynthetic antenna complexes and light harvesting nanotubes.[1,49] The energy concentration from large area 2D to 0D semiconductors of the same composition, however, has not been previously explored to our knowledge. It has been shown from 2D TMDs to separately synthesized nanocrystals such as WS_2 to PbS-CdS, WS_2 to CdSe/ZnS, and MoS_2 to CdSeTe/ZnS, as well as in InGaAs quantum wells to CdSe/ZnS QDs.[3,43,44,50] In NPLs, energy transfer from 2D to 0D has been demonstrated from CdSe NPL to metallic nanoparticles such as Pt, Pd, and Au.[18,45,51,52] Similarly, energy transfer from 2D NPLs to molecular chromophores has been demonstrated such as in 3 ML CdSe NPLs to conjugated fluorophores.[46] These results are summarized in Figure 5b, where the QE is shown as a function of acceptor density (or the number of reported acceptors per area of donor). In these systems, energy transfer is dominated by FRET and is limited by spectral overlap, distance from donor to acceptor, and high concentrations needed which may induce self-quenching. Our system overcomes all these limitations by having tunable spectral overlap, epitaxial contact between donor and acceptor, and extremely low concentrations of acceptor relative to donor. Together these results all highlight the efficiency of this system for infrared energy concentration using a minimal amount of material and demonstrate its promise in applications such as solar concentration.

Overall, we observe that HgTe NPLs can act as highly efficient energy antennas to HgTe QDs with bandgaps in the shortwave infrared. The energy transfer is highest when the QDs are grown in situ from the excess precursors in solution during cation exchange. We evaluate the energy transfer of this system to be near unity and determine that excitons within NPLs must diffuse a large area before reaching the QD, and the exciton diffusion constant is higher than that reported for other nanocrystals. These results both highlight the similarities between NPLs and extended 2D semiconductors such as transition metal dichalcogenides and provide a promising platform for infrared energy collection and concentration.

■ ASSOCIATED CONTENT

Supporting Information

The Supporting Information is available free of charge at https://pubs.acs.org/doi/10.1021/acs.jpclett.3c02168.

Experimental details and methods, additional characterization through absorbance and photoluminescence, photoluminescence lifetimes, details on calculations and modeling (PDF)

■ AUTHOR INFORMATION

Corresponding Author

Justin R. Caram − *Department of Chemistry and Biochemistry, University of California, Los Angeles, California 90095-1569, United States;* orcid.org/0000-0001-5126-3829; Email: jcaram@chem.ucla.edu

Authors

Stephanie M. Tenney − *Department of Chemistry and Biochemistry, University of California, Los Angeles, California 90095-1569, United States;* orcid.org/0000-0001-7749-9944

Lauren A. Tan − *Department of Chemistry and Biochemistry, University of California, Los Angeles, California 90095-1569, United States*

Xuanheng Tan − *Department of Chemistry and Biochemistry, University of California, Los Angeles, California 90095-1569, United States*

Mikayla L. Sonnleitner − *Department of Chemistry and Biochemistry, University of California, Los Angeles, California 90095-1569, United States*

Belle Coffey − *Department of Chemistry and Biochemistry, University of California, Los Angeles, California 90095-1569, United States*

Jillian A. Williams − *Department of Chemistry and Biochemistry, University of California, Los Angeles, California 90095-1569, United States*

Ricky Ronquillo − *Department of Chemistry and Biochemistry, University of California, Los Angeles, California 90095-1569, United States*

Timothy L. Atallah − *Department of Chemistry and Biochemistry, Denison University, Granville, Ohio 43023, United States;* orcid.org/0000-0003-2863-6601

Tasnim Ahmed − *Department of Chemistry and Biochemistry, University of California, Los Angeles, California 90095-1569, United States*

Complete contact information is available at: https://pubs.acs.org/10.1021/acs.jpclett.3c02168

Author Contributions

[§]S.M.T. and L.A.T. contributed equally to this paper. S.M.T. and L.A.T. conducted all synthesis, characterization, and calculations of Q.E., assisted by M.L.S. X.T. modeled FRET rates and calculations of distance dependence. S.M.T. modeled the exciton diffusion constant. B.C. and R.R. assisted with collecting additional absorbance and photoluminescence. J.A.W. collected TEM images. T.L.A., T.A., and J.R.C. provided mentorship and guidance.

Funding

This work was supported by the National Science Foundation Career Award No. 1945572.

Notes

The authors declare no competing financial interest.

■ ACKNOWLEDGMENTS

We would like to thank Professor Ellen Sletten and the Materials Characterization Laboratory at UCLA for their instrumentation. The authors acknowledge the use of instruments at the Electron Imaging Center for NanoMachines supported by NIH (1S10RR23057, 1S10OD018111 and 1U24GM116792), NSF (DBI-1338135) and CNSI at UCLA.

■ REFERENCES

(1) Freyria, F. S.; Cordero, J. M.; Caram, J. R.; Doria, S.; Dodin, A.; Chen, Y.; Willard, A. P.; Bawendi, M. G. Near-Infrared Quantum Dot Emission Enhanced by Stabilized Self-Assembled J-Aggregate Antennas. *Nano Lett.* **2017**, *17*, 7665−7674.
(2) Zhang, Q.; Atay, T.; Tischler, J. R.; Bradley, M. S.; Bulović, V.; Nurmikko, A. V. Highly Efficient Resonant Coupling of Optical Excitations in Hybrid Organic/Inorganic Semiconductor Nanostructures. *Nat. Nanotechnol.* **2007**, *2*, 555−559.
(3) Tanoh, A. O. A.; Gauriot, N.; Delport, G.; Xiao, J.; Pandya, R.; Sung, J.; Allardice, J.; Li, Z.; Williams, C. A.; Baldwin, A.; Stranks, S. D.; Rao, A. Directed Energy Transfer from Monolayer WS2 to Near-Infrared Emitting PbS−CdS Quantum Dots. *ACS Nano* **2020**, *14*, 15374−15384.
(4) Sundström, V.; Pullerits, T.; Van Grondelle, R. Photosynthetic Light-Harvesting: Reconciling Dynamics and Structure of Purple Bacterial LH2 Reveals Function of Photosynthetic Unit. *J. Phys. Chem. B* **1999**, *103*, 2327−2346.
(5) Scholes, G. D.; Rumbles, G. Excitons in Nanoscale Systems. *Nat. Mater.* **2006**, *5*, 683−696.
(6) Cnops, K.; Rand, B. P.; Cheyns, D.; Verreet, B.; Empl, M. A.; Heremans, P. 8.4% Efficient Fullerene-Free Organic Solar Cells Exploiting Long-Range Exciton Energy Transfer. *Nat. Commun.* **2014**, *5*, 1−6.
(7) Ithurria, S.; Tessier, M. D.; Mahler, B.; Lobo, R. P. S. M.; Dubertret, B.; Efros, A. L. Colloidal Nanoplatelets with Two-Dimensional Electronic Structure. *Nat. Mater.* **2011**, *10*, 936−941.
(8) Yeltik, A.; Delikanli, S.; Olutas, M.; Kelestemur, Y.; Guzelturk, B.; Demir, H. V. Experimental Determination of the Absorption Cross-Section and Molar Extinction Coefficient of Colloidal CdSe Nanoplatelets. *J. Phys. Chem. C* **2015**, *119*, 26768−26775.
(9) Hu, A.; Bai, P.; Zhu, Y.; Song, Z.; Wang, R.; Zheng, J.; Yao, Y.; Zhang, Q.; Ding, Z.; Gao, P.; Sui, X.; Liu, X.; Gao, Y. Green CdSe/CdSeS Core/Alloyed-Crown Nanoplatelets Achieve Unity Photoluminescence Quantum Yield over a Broad Emission Range. *Adv. Opt. Mater.* **2022**, *10*, 2200469.
(10) Scott, R.; Heckmann, J.; Prudnikau, A. V.; Antanovich, A.; Mikhailov, A.; Owschimikow, N.; Artemyev, M.; Climente, J. I.; Woggon, U.; Grosse, N. B.; Achtstein, A. W. Directed Emission of CdSe Nanoplatelets Originating from Strongly Anisotropic 2D Electronic Structure. *Nat. Nanotechnol.* **2017**, *12*, 1155−1160.
(11) Tenney, S. M.; Tan, L. A.; Sonnleitner, M. L.; Sica, A. V.; Shin, A. J.; Ronquillo, R.; Ahmed, T.; Atallah, T. L.; Caram, J. R. Mesoscale Quantum-Confined Semiconductor Nanoplatelets through Seeded Growth. *Chem. Mater.* **2022**, *34*, 6048−6056.
(12) Izquierdo, E.; Dufour, M.; Chu, A.; Livache, C.; Martinez, B.; Amelot, D.; Patriarche, G.; Lequeux, N.; Lhuillier, E.; Ithurria, S. Coupled HgSe Colloidal Quantum Wells through a Tunable Barrier: A Strategy to Uncouple Optical and Transport Band Gap. *Chem. Mater.* **2018**, *30*, 4065−4072.
(13) Izquierdo, E.; Robin, A.; Keuleyan, S.; Lequeux, N.; Lhuillier, E.; Ithurria, S. Strongly Confined HgTe 2D Nanoplatelets as Narrow Near-Infrared Emitters. *J. Am. Chem. Soc.* **2016**, *138*, 10496−10501.
(14) Tenney, S. M.; Vilchez, V.; Sonnleitner, M. L.; Huang, C.; Friedman, H. C.; Shin, A. J.; Atallah, T. L.; Deshmukh, A. P.; Ithurria, S.; Caram, J. R. Mercury Chalcogenide Nanoplatelet−Quantum Dot Heterostructures as a New Class of Continuously Tunable Bright Shortwave Infrared Emitters. *J. Phys. Chem. Lett.* **2020**, *11*, 3473−3480.
(15) Horani, F.; Meir, I.; Lifshitz, E. Room Temperature Colloidal Coating of II−VI Nanoplatelets with Quantum Dots. *J. Phys. Chem. C* **2021**, *125*, 25729−25738.
(16) Williams, K. R.; Diroll, B. T.; Watkins, N. E.; Rui, X.; Brumberg, A.; Klie, R. F.; Schaller, R. D. Synthesis of Type i PbSe/CdSe Dot-on-Plate Heterostructures with Near-Infrared Emission. *J. Am. Chem. Soc.* **2019**, *141*, 5092−5096.
(17) Salzmann, B. B.V.; de Wit, J.; Li, C.; Arenas-Esteban, D.; Bals, S.; Meijerink, A.; Vanmaekelbergh, D. Two-Dimensional CdSe-PbSe Heterostructures and PbSe Nanoplatelets: Formation, Atomic Structure, and Optical Properties. *J. Phys. Chem. C* **2022**, *126*, 1513−1522.
(18) Medda, A.; Dutta, A.; Bain, D.; Mohanta, M. K.; De Sarkar, A.; Patra, A. Electronic Structure Modulation of 2D Colloidal CdSe Nanoplatelets by Au25 Clusters for High-Performance Photodetectors. *J. Phys. Chem. C* **2020**, *124*, 19793−19801.
(19) Piepenbrock, M.-O. M.; Stirner, T.; Kelly, S. M.; O'Neill, M. O'Neill, M.A Low-Temperature Synthesis for Organically Soluble HgTe Nanocrystals Exhibiting near-Infrared Photoluminescence and Quantum Confinement. *J. Am. Chem. Soc.* **2006**, *128*, 7087−7090.
(20) Lindsey, J. S.; Taniguchi, M.; Bocian, D. F.; Holten, D. The Fluorescence Quantum Yield Parameter in Förster Resonance Energy Transfer (FRET)—Meaning, Misperception, and Molecular Design. *Chem. Phys. Rev.* **2021**, *2*, 2.
(21) Chuang, C.; Knoester, J.; Cao, J. Scaling Relations and Optimization of Excitonic Energy Transfer Rates between One-Dimensional Molecular Aggregates. *J. Phys. Chem. B* **2014**, *118*, 7827−7834.
(22) Yuan, L.; Wang, T.; Zhu, T.; Zhou, M.; Huang, L. Exciton Dynamics, Transport, and Annihilation in Atomically Thin Two-Dimensional Semiconductors. *J. Phys. Chem. Lett.* **2017**, *8*, 3371−3379.
(23) Lee, E. M. Y.; Tisdale, W. A. Determination of Exciton Diffusion Length by Transient Photoluminescence Quenching and Its Application to Quantum Dot Films. *J. Phys. Chem. C* **2015**, *119*, 9005−9015.
(24) Akselrod, G. M.; Prins, F.; Poulikakos, L. V.; Lee, E. M. Y.; Weidman, M. C.; Mork, A. J.; Willard, A. P.; Bulovic, V.; Tisdale, W. A. Exciton Transport in Quantum Dot Solids. *Nano Lett.* **2014**, *14*, 3556−3562.
(25) Yoon, S. J.; Guo, Z.; dos Santos Claro, P. C.; Shevchenko, E. V.; Huang, L. Direct Imaging of Long-Range Exciton Transport in Quantum Dot Superlattices by Ultrafast Microscopy. *ACS Nano* **2016**, *10*, 7208−7215.
(26) Penzo, E.; Loiudice, A. S.; Barnard, E. J.; Borys, N. J.; Jurow, M.; Lorenzon, M.; Rajzbaum, I. K.; Wong, E.; Liu, Y. M.; Schwartzberg, A.; Cabrini, S.; Whitelam, S.; Buonsanti, R.; Weber-Bargioni, A. Long-Range Exciton Diffusion in Two-Dimensional Assemblies of Cesium Lead Bromide Perovskite Nanocrystals. *ACS Nano* **2020**, *14*, 6999−7007.
(27) Mikhnenko, O. V.; Cordella, F.; Sieval, A. B.; Hummelen, J. C.; Blom, P. W. M.; Loi, M. A. Temperature Dependence of Exciton Diffusion in Conjugated Polymers. *J. Phys. Chem. B* **2008**, *112*, 11601−11604.
(28) Lewis, A. J.; Ruseckas, A.; Gaudin, O. P. M.; Webster, G. R.; Burn, P. L.; Samuel, I. D. W. Singlet Exciton Diffusion in MEH-PPV Films Studied by Exciton-Exciton Annihilation. *Org. Electron.* **2006**, *7*, 452−456.
(29) Zhu, T.; Wan, Y.; Guo, Z.; Johnson, J.; Huang, L. Two Birds with One Stone: Tailoring Singlet Fission for Both Triplet Yield and Exciton Diffusion Length. *Adv. Mater.* **2016**, *28*, 7539−7547.
(30) Hertel, T.; Himmelein, S.; Ackermann, T.; Stich, D.; Crochet, J. Diffusion Limited Photoluminescence Quantum Yields in 1-D Semiconductors: Single-Wall Carbon Nanotubes. *ACS Nano* **2010**, *4*, 7161−7168.
(31) Yoshikawa, K.; Matsuda, K.; Kanemitsu, Y. Exciton Transport in Suspended Single Carbon Nanotubes Studied by Photoluminescence Imaging Spectroscopy. *J. Phys. Chem. C* **2010**, *114*, 4353−4356.

https://doi.org/10.1021/acs.jpclett.3c02168
J. Phys. Chem. Lett. 2023, 14, 9456−9463

(32) Caram, J. R.; Doria, S.; Eisele, D. M.; Freyria, F. S.; Sinclair, T. S.; Rebentrost, P.; Lloyd, S.; Bawendi, M. G. Room-Temperature Micron-Scale Exciton Migration in a Stabilized Emissive Molecular Aggregate. *Nano Lett.* **2016**, *16*, 6808−6815.
(33) Deng, S.; Shi, E.; Yuan, L.; Jin, L.; Dou, L.; Huang, L. Long-Range Exciton Transport and Slow Annihilation in Two-Dimensional Hybrid Perovskites. *Nat. Commun.* **2020**, *11*, 664.
(34) Seitz, M.; Magdaleno, A. J.; Alcázar-Cano, N.; Meléndez, M.; Lubbers, T. J.; Walraven, S. W.; Pakdel, S.; Prada, E.; Delgado-Buscalioni, R.; Prins, F. Exciton Diffusion in Two-Dimensional Metal-Halide Perovskites. *Nat. Commun.* **2020**, *11*, 2035.
(35) Yu, Y.; Yu, Y.; Li, G.; Puretzky, A. A.; Geohegan, D. B.; Cao, L. Giant Enhancement of Exciton Diffusivity in Two-Dimensional Semiconductors. *Sci. Adv.* **2020**, *6*, 4823−4841.
(36) Javey, A.; Uddin, S. Z.; Kim, H.; Lorenzon, M.; Yeh, M.; Lien, D. H.; Barnard, E. S.; Htoon, H.; Weber-Bargioni, A. Neutral Exciton Diffusion in Monolayer MoS2. *ACS Nano* **2020**, *14*, 13433−13440.
(37) Rosati, R.; Brem, S.; Perea-Causin, R.; Schmidt, R.; Niehues, I.; Michaelis De Vasconcellos, S.; Bratschitsch, R.; Malic, E. Strain-Dependent Exciton Diffusion in Transition Metal Dichalcogenides. *2D Mater.* **2021**, *8*, 015030.
(38) Chen, P.; Atallah, T. L.; Lin, Z.; Wang, P.; Lee, S. J.; Xu, J.; Huang, Z.; Duan, X.; Ping, Y.; Huang, Y.; Caram, J. R.; Duan, X. Approaching the Intrinsic Exciton Physics Limit in Two-Dimensional Semiconductor Diodes. *Nat.* **2021**, *599*, 404−410.
(39) Kumar, N.; Cui, Q.; Ceballos, F.; He, D.; Wang, Y.; Zhao, H. Exciton Diffusion in Monolayer and Bulk MoSe2. *Nanoscale* **2014**, *6*, 4915−4919.
(40) Cadiz, F.; Robert, C.; Courtade, E.; Manca, M.; Martinelli, L.; Taniguchi, T.; Watanabe, K.; Amand, T.; Rowe, A. C. H.; Paget, D.; Urbaszek, B.; Marie, X. Exciton Diffusion in WSe2Monolayers Embedded in a van Der Waals Heterostructure. *Appl. Phys. Lett.* **2018**, *112*, 152106.
(41) Achtstein, A. W.; Ayari, S.; Helmrich, S.; Quick, M. T.; Owschimikow, N.; Jaziri, S.; Woggon, U. Tuning Exciton Diffusion, Mobility and Emission Line Width in CdSe Nanoplatelets via Lateral Size. *Nanoscale* **2020**, *12*, 23521−23531.
(42) Li, Q.; Wu, K.; Chen, J.; Chen, Z.; McBride, J. R.; Lian, T. Size-Independent Exciton Localization Efficiency in Colloidal CdSe/CdS Core/Crown Nanosheet Type-I Heterostructures. *ACS Nano* **2016**, *10*, 3843−3851.
(43) Li, B.; Gao, Y.; Wu, R.; Miao, X.; Zhang, G. Charge and Energy Transfer Dynamics in Single Colloidal Quantum Dots/Monolayer MoS2 Heterostructures. *Phys. Chem. Chem. Phys.* **2023**, *25*, 8161−8167.
(44) Achermann, M.; Petruska, M. A.; Kos, S.; Smith, D. L.; Koleske, D. D.; Klimov, V. I. Energy-Transfer Pumping of Semiconductor Nanocrystals Using an Epitaxial Quantum Well. *Nature* **2004**, *429*, 642−646.
(45) Wu, K.; Li, Q.; Du, Y.; Chen, Z.; Lian, T. Ultrafast Exciton Quenching by Energy and Electron Transfer in Colloidal CdSe Nanosheet−Pt Heterostructures. *Chem. Sci.* **2015**, *6*, 1049−1054.
(46) Halim, H.; Trieb, D.; Huber, N.; Martínez-Negro, M.; Meyer, L.-A.; Basché, T.; Morsbach, S. A. I.; Zhang, K.; Riedinger, A. Lateral Size Dependence in FRET between Semiconductor Nanoplatelets and Conjugated Fluorophores. *J. Phys. Chem. C* **2020**, *124*, 25028−25037.
(47) Yuan, L.; Huang, L. Exciton Dynamics and Annihilation in WS2 2D Semiconductors. *Nanoscale* **2015**, *7*, 7402−7408.
(48) Amani, M.; Lien, D.-H.; Kiriya, D.; Xiao, J.; Azcatl, A.; Noh, J.; Madhvapathy, S. R.; Addou, R.; KC, S.; Dubey, M.; Cho, K.; Wallace, R. M.; Lee, S.-C.; He, J.-H.; Ager, J. W.; Zhang, X.; Yablonovitch, E.; Javey, A. Near-Unity Photoluminescence Quantum Yield in MoS2. *Science* **2015**, *350*, 1065−1068.
(49) Mirkovic, T.; Ostroumov, E. E.; Anna, J. M.; van Grondelle, R.; Govindjee; Scholes, G. D. Light Absorption and Energy Transfer in the Antenna Complexes of Photosynthetic Organisms. *Chem. Rev.* **2017**, *117*, 249−293.
(50) Boulesbaa, A.; Wang, K.; Mahjouri-Samani, M.; Tian, M. A.; Puretzky, A.; Ivanov, I. M.; Rouleau, C.; Xiao, K. G.; Sumpter, B. B.; Geohegan, D. Ultrafast Charge Transfer and Hybrid Exciton Formation in 2D/0D Heterostructures. *J. Am. Chem. Soc.* **2016**, *138*, 14713−14719.
(51) Mahler, B.; Guillemot, L.; Bossard-Giannesini, L.; Ithurria, S.; Pierucci, D.; Ouerghi, A.; Patriarche, G.; Benbalagh, R.; Lacaze, E.; Rochet, F.; Lhuillier, E. Metallic Functionalization of CdSe 2D Nanoplatelets and Its Impact on Electronic Transport. *J. Phys. Chem. C* **2016**, *120*, 12351−12361.
(52) Naskar, S.; Schlosser, A.; Miethe, J. F.; Steinbach, F.; Feldhoff, A.; Bigall, N. C. Site-Selective Noble Metal Growth on CdSe Nanoplatelets. *Chem. Mater.* **2015**, *27*, 3159−3166.

https://doi.org/10.1021/acs.jpclett.3c02168
J. Phys. Chem. Lett. 2023, 14, 9456−9463